1. Introduction

Forests play a critical role in regulating the global hydrological and carbon cycles (Dixon et al. 1994; Pan et al. 2013). Globally, drought has been identified as the most widespread stress factor that pushes trees to their physiological threshold and causes irreversible damage (Allen et al. 2010; McDowell et al. 2008). Recently, Europe has experienced frequent devastating droughts and heatwaves, which have led to increased concern regarding the stability of local forest ecosystems and regional carbon cycles (Ciais et al. 2005; Fischer et al. 2010; Schär et al. 2004; Seneviratne et al. 2006; Zaitchik et al. 2006). European productive temperate forests have been significantly affected by these extreme drought events, and it is estimated that the droughts caused a mean reduction in net primary productivity (NPP) of 16 gC m–2 month–1 in the summer of 2003 (Ciais et al. 2005). More frequent droughts can be expected as the climate warms (Meehl et al. 2004; Schär et al. 2004). Therefore, understanding the resistance of forests to drought is critical if we are to accurately forecast future forest dynamics in Europe.

Previous studies have reported a height-dependence with respect to the resistance of forests to drought (Bennett et al. 2015; Lindenmayer et al. 2012; Lutz et al. 2012; Phillips et al. 2010). It has been suggested that, under drought conditions in Europe, tall vegetation experiences relatively less browning and a smaller reduction in gross primary productivity (GPP), which indicates less water stress and drought impacts on tall vegetation (Bevan et al. 2014). However, some other studies indicate large trees are more likely than small trees to succumb to extreme drought (Bennett et al. 2015; McDowell et al. 2015). For example, large trees die at twice the rate of small trees in conifer-dominated forest in the Southwest of North America from 2009 to 2016 (Stovall et al. 2019, 2020). These findings are surprising, and it is unclear why large trees experience less variability in greenness during drought, but have a higher risk of

drought-associated mortality than small trees. This highlights our limited understanding of the height-dependent resistance of vegetation to drought.

Base on the satellite vegetation index data, canopy height data and the meteorological data, we comprehensively explore the variations in height-dependence of the drought resistance of forests through the evolution of a drought by dividing the European 2003 and 2018 droughts into three stages: the early, aggregating, and recovery stages. The specific aims of this paper are to: 1) evaluate the vegetation greenness anomalies of trees in different height across the three stages of the 2003 and 2018 drought events; and 2) investigate the potential mechanisms responsible for the differences in drought resistance among trees of different height by examining their physiological traits, including root depth, stomatal regulation, and sapflow density.

2. Material and methods

2.1 Data

The monthly 2-m air temperature data and volumetric soil water content (SWV; at depths of 0–7, 7–28, 28–100, and 100–289 cm) with a 0.1° × 0.1° spatial resolution for the period 2001–2018 were obtained from the ERA5 dataset provided by the European Centre for Medium Range Weather Forecasts (ECMWF: https://cds.climate.copernicus.eu/#!/search?text=ERA5&type=dataset). The original Kelvin (K) unit of temperature from ERA5 was converted to Centigrade (°C) for ease of reading. We also obtained global monthly precipitation data for the period 2001–2018, which has a spatial resolution of 0.5° × 0.5°, from the Climate Research Unit (CRU) Time Series 4.03 dataset. (http://data.ceda.ac.uk// badc/cru/).

The vegetation status under drought was derived from the Moderate Resolution Imaging Spectroradiometer (MODIS) normalized difference vegetation index (NDVI) and the enhanced vegetation index (EVI; http://modis.gsfc.nasa.gov/) with a spatial resolution of 0.05° × 0.05° and a monthly temporal resolution.

The forest canopy height dataset was obtained from the NASA Carbon Monitoring System (CMS) program. This dataset provides estimates of forest canopy height derived from the Geoscience Laser Altimeter System (GLAS) LiDAR instrument that onboard the NASA Ice, Cloud, and land Elevation (ICESat) satellite (Healey et al. 2016; Lefsky et al. 2007). In total, we analyzed observations from 4727 forested sites across Europe. Canopy height data points were sampled according to European biogeography regions, as defined by the European Environment Agency (EEA, https://www.eea.europa.eu/data-and-maps/figures/biogeographical-regions-in-europe-2) on the basis of climate, topography, and vegetation, which are widely accepted (Painho et al. 1996).

The global maximum rooting depth dataset, which has a 1-km spatial resolution, was provided by Fan et al. (2017). This dataset is based on the inversion of an ecohydrological model combined with water table estimates, and has been extensively validated by field observations (Fig. S7).

The sapflow dataset was obtained from SAPFLUXNET (https://zenodo.org/record/3697807#. Xs4yo4gza5u), which is a compiled global plant-level sap flow measurement database. Two observing sites with similar climatic conditions and tree species (*Fagus sylvatica*), but significantly different tree heights, were used, namely: site DEU_STE_2P3 in Germany (Lüttschwager et al. 2007) and site FRA_HES_HE2_NON in France (Bovard et al. 2005).

The global forest isohydricity metric dataset, which is calculated from the long-term diurnal variations in microwave vegetation optical depth and is dependent on vegetation water content, has a spatial resolution of 0.25° × 0.25° and was obtained from Konings et al. (2017).

2.2 Methods

2.2.1 Climate and vegetation anomalies calculation

To calculate anomalies in temperature, precipitation, and volumetric soil water (SWV), as well as the vegetation indexes NDVI and EVI, during the drought events, the reference state was defined as the arithmetical mean for each month over the period 2001–2018 (excluding the drought years of 2003 and 2018). The anomalies for each indicator were determined using the current month values relative to the reference state, an approach that is frequently used in drought studies (Ji et al. 2003; Kogan, 1995, 1997; Liu et al. 1996; Peters et al. 2002).

2.2.2 Sampling methods

The drought years of 2003 and 2018 experienced prolonged precipitation deficits and record-breaking high temperatures that seriously affected forest activity and biomass production across Europe. We used three steps to generate the data points of canopy heights and other parameters used in our analysis of these two drought-affected years.

Step I: We first selected forests sites with height observations in the drought-affected areas that experienced temperature anomalies greater than 2°C and precipitation anomalies of less than 0 mm (Liu et al. 2020). Totally 1076 canopy height samples in 2003 and 645 in 2018 from these forests were selected in this step.

Step II: A critical prerequisite for exploring the differences in resistance to drought among a variety of canopy heights is to ensure that the comparisons are made under nearly the same climatic conditions. Therefore, the forests were next sampled using the European Environment Agency (EEA) biogeography regions. This division is appropriate across Europe because these zones are defined on the basis of climate, topography, and potential vegetation, and are best interpreted as areas of relatively homogeneous ecological conditions, within which comparisons and assessments of vegetation–climate feedback are meaningful (Painho et al. 1996). A further 453 canopy height samples were selected in 2003 and 436 in 2018.

Step III: We used a sampling method based on a greedy algorithm (Vince 2002) that guarantees the maximum forest sites size but removes any existing correlations between canopy heights and climatic variables. The basic idea of sample method is to proceed step by step from a certain initial solution of the problem. According to some optimization measure, each step must ensure that the local optimal solution can be obtained. Only one data is considered in each step, and its selection should satisfy the conditions of local optimization. If the next data and the partial optimal solution are no longer feasible, the data is not added to the partial solution. The algorithm doesn't stop until all data is enumerated. Detailed information related to this sampling method can be found in Text S1 and Fig. S2 of the supplementary information. We ultimately selected 397 and 393 canopy height samples for analysis from 2003 and 2018, respectively (Fig. S3).

2.2.3 Statistical analysis

Among the selected forest sites, the corresponding climatologic and vegetation variables were extracted and grouped into 1-m increments of forest canopy height. Then,

a linear regression model was built to test whether the vegetation greenness anomalies varied with canopy height during the drought events. The reliability of the regression models was examined using a *t* test at a significance level of 0.05.

In addition, we measured the intra-group difference in vegetation greenness anomalies and soil water content anomalies along with the drought development process by grouping canopy heights into <10, 10–20, 20–30, and >30 m. The intra-group differences were examined using a *t* test at a significance level of 0.05.

3. Results

3.1 Height-dependent resistance to drought

An intense and widespread drought influenced central Europe in August 2003 with maximum positive temperature anomalies reaching 6.1°C and maximum negative precipitation anomalies of approximately 101.4 mm (Fig. S5). These dry and hot conditions gave rise to a rapid shift in vegetation color from green to brown across central Europe in August (Liberto 2018). About 98.7% of samples from 2003 showed negative NDVI anomalies, and the largest decrease in NDVI was observed in central France in 2003. In contrast, the drought in August 2018 exhibited lower temperature anomalies (4.1°C) but a more pronounced precipitation deficiency (122.5 mm) in central Europe (Liu et al. 2020). About 91.2% of samples from 2018 showed negative NDVI anomalies, and the largest anomalies were observed in eastern Germany (Fig. 1a, c).

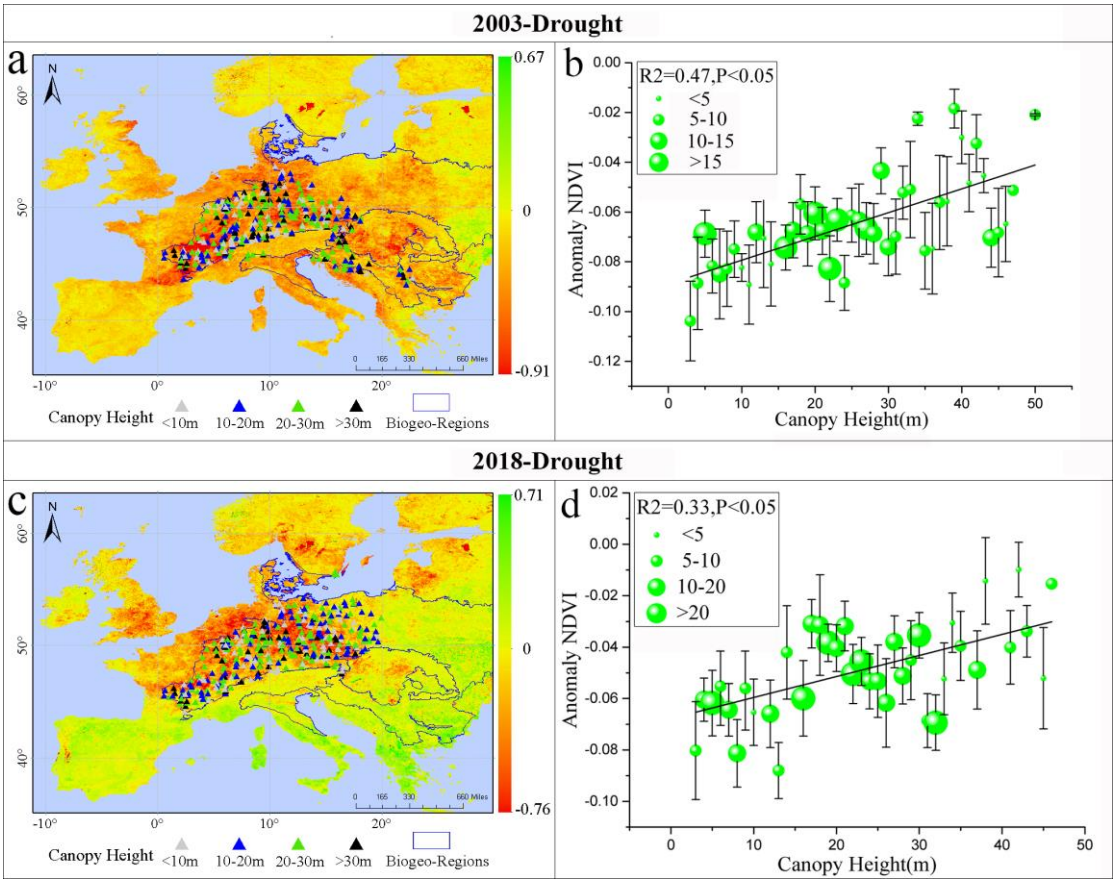

138

139 **Fig. 1 Anomalies in MODIS NDVI and variations binned by tree height. (a, c)**
140 NDVI anomalies in August 2003 and August 2018. The anomalies are relative to the
141 reference state defined as the mean values over the period 2001–2018 (excluding 2003
142 and 2018). The colored triangles indicate trees of different heights (<10, 10–20, 20–30,
143 and >30 m). **(b, d)** The relationship between NDVI anomalies and tree height grouped
144 at each 1-m height for August 2003 (397 Samples) and August 2018 (393 Samples).
145 The green dot size reflects the number of sample points in each height class. Error bars
146 indicate standard deviations. The significance of the relationship was examined using a
147 *t* test at a significance level of 0.05.

148 During both drought events, negative NDVI anomalies are obvious and cover large
149 areas of central Europe, where conifer forests are dominant (Fig. 1a, c). A significant
150 positive relationship between canopy height and NDVI anomalies is observed in both
151 2003 ($R2 = 0.47$, $p < 0.05$) and 2018 ($R2 = 0.33$, $p < 0.05$; Fig. 1b, d), which indicates
152 that short trees experienced more browning than tall trees and thereby have a lower
153 resistance to drought. For every 10 m the trees grew, the average NDVI anomalies
154 decreased by approximately 1.35% and 1.26%, in 2003 and 2018, respectively. We used
155 the EVI dataset to validate these relationships and obtained similar results, although the

R2 values were slightly smaller (Fig. S4, R2 = 0.37 and 0.28 for 2003 and 2018, respectively). This observed height-dependence of the resistance of trees to drought is supported by previous work that suggested a regionally coherent positive correlation between tree height and NDVI anomalies across eastern France and most of Germany (Bevan et al. 2014).

3.2 Temporal evolution of height-dependent resistance to drought.

We extended our investigation of the meteorological and vegetation conditions to reveal the drought evolution process and track variations in the resistance of the trees to water deficiency in different heights. Trees from the drought-affected areas were binned into four groups according to canopy height (<10, 10–20, 20–30, and >30 m) for convenience of comparison (Fig. 2a, c). It is clear that both drought events were preceded by a warm and dry spring (early stage: I), then the persistent increasing temperature and decreasing precipitation developed into a serious summer drought (aggravating stage: II), and finally temperature and precipitation returned to normal climatic levels (recovery stage: III) indicating the end of the drought events and vegetation recovery.

Generally, NDVI changes followed a similar temporal evolution but with differing fluctuation amplitudes during both drought events. Positive NDVI anomalies are observed from May to June in most areas indicating the brief green-up occurring in the warm spring (Figs 2a, b and S5a, b, h, i), in consistent with the previous report (Zaitchik et al. 2006). The maximum NDVI anomalies occurred in May, with 1.6% in 2003 and 3.1% in 2018 (Table S1). Spring vegetation green-up enhanced evapotranspiration, and thereby contributed to rapid soil drying (Bevan et al. 2014; García-Herrera et al. 2010; Zaitchik et al. 2006), and consequently caused the dramatic browning of vegetation in

the summer (Fig. S5). Owing to the soil moisture deficit (Garciaherrera et al. 2010), the most serious forest browning was observed in August, with maximum NDVI anomalies of –6.6% in 2003 and –5.1% in 2018 (Table S1). Finally, the forest began to recover as the temperature and precipitation returned to normality after both events (Fig. 2a, c). The average NDVI anomalies of the forest sites studied had rebounded to –1.1% and –2.5% in October of 2003 and 2018, respectively (Table S1).

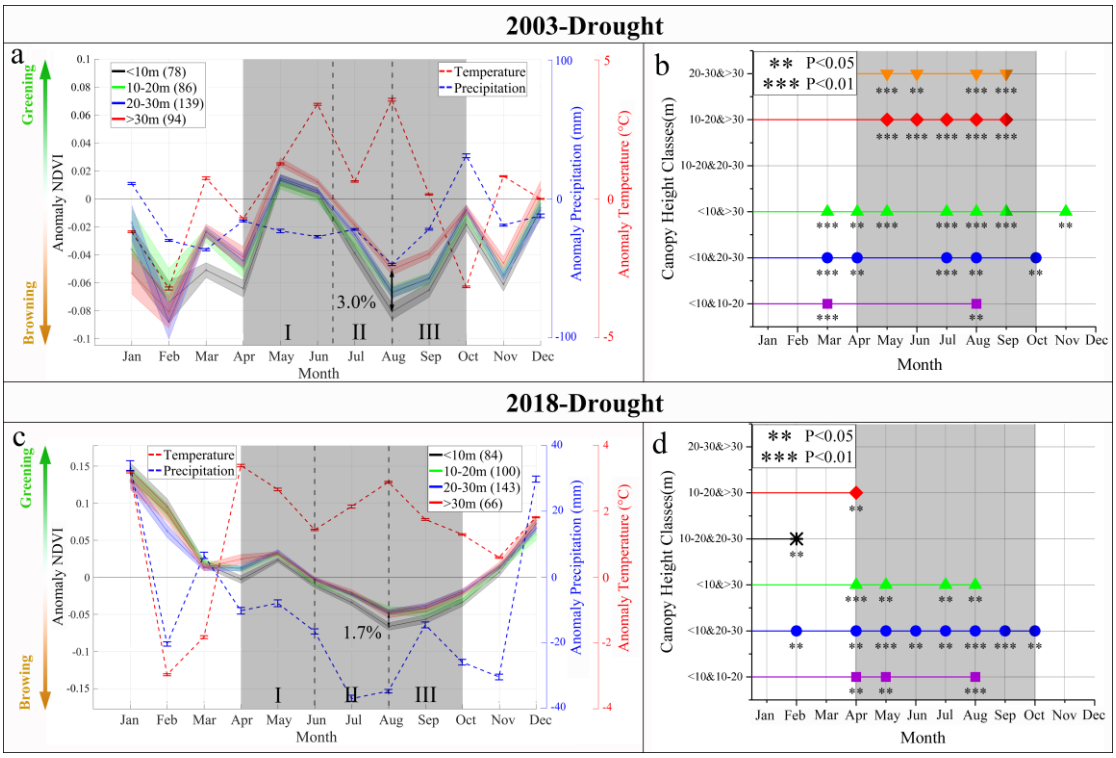

Fig. 2 a, c Average air temperature anomalies (red dashed line), precipitation anomalies (blue dashed line), and NDVI anomalies for the four height classes relative to the 2001–2018 average (excluding 2003 and 2018) for the time series from 2003 and 2018: <10 m (black solid line); 10–20 m (green solid line); 20–30 m (blue solid line); >30 m (red solid line). Error bars and shaded error regions around each curve are standard deviations **b, d Differences in NDVI anomalies between different height classes.** Different symbols represent different height class groups. The significance of the difference was calculated using a *t* test with a significance level of 0.05 (**) and 0.01 (***). Gray shaded regions show the duration (April to October) of drought in 2003 and 2018.

Obvious differences in the greenness response of the trees is evident among the various height groups throughout the development of the drought events, which suggests that the height-dependent drought resistance of the trees persisted throughout the drought

events. Taller trees generally showed more greening in the early stage, less browning in the aggravating stage, and also less re-greening in the recovery stage. For instance, the maximum anomalies of NDVI variations are 5.1% for trees >30 m in aggravating stages of the 2003 drought, in contrast to 8.1% for tree <10 m (Fig. 2a, c). This phenomenon can also be observed for the drought event of 2018; i.e., 6.6% and 4.9% for trees <10 and >30 m, respectively (Table S1).

We also conducted a pairwise comparison to further test the group differences during the drought evolution process (Fig. 2b, d). Trees over 30 m tall and those less than 10 m tall show the most obvious differences when compared with trees from the other groups. Throughout all stages of the two drought events, we observed significant differences between NDVI anomalies of trees <10 m and the other groups of trees. For trees >30 m, the significant differences are found with <10m, 10-20m, 20-30m groups in 2003 but only with <10m group in 2018. The smallest NDVI anomaly gap exists between trees of 10–20 m and those of 20–30 m (Fig. 2b, d). Generally, trees undergo significant changes in size, growth form, and physiology as they proceed from seedlings to maturity further to old age. These changes significantly affect hydraulic conductance and photosynthesis, and consequently show significant greenness differences during droughts (Hubbard et al. 1999; Nepstad et al. 2007; Ryan et al. 1997; Ryan & Yoder 1997; Xu et al. 2018; Zhang et al. 2009).

Although similar drought development processes were clear in both 2003 and 2018, we found that smaller forest group differences in the NDVI anomalies occurred during the extreme drought stage of 2018 (1.7%) than in 2003 (3.0%). Correspondingly, the differences among the 10–20, 20–30, and >30 m groups were less significant during all stages of the drought in 2018 (Fig. 2b, d). This may suggest that the more severe the drought, the more pronounced the height-dependent tree resistance (Bevan et al. 2014;

225 Xu et al. 2018). However, this would need to be demonstrated in more drought events
226 with varying intensity.

227 **3.3 Height-dependence of tree's hydraulic absorption behavior to drought**

228 Soil water deficiency is the fundamental cause of tree browning during droughts
229 (Fischer et al. 2007; Liu et al. 2020). Here, we used the anomalies in volume of water
230 in four soil layers (covering depths of 0–7, 7–28, 28–100, and 100–289 cm) to represent
231 the soil water deficiency during the droughts of 2003 and 2018 (Fig. 3a, c). We found
232 that the deep soil water profiles slowly and steadily declined during the drought
233 evolution process. For example, the soil layer at 100–289 cm began to show a hydraulic
234 deficiency in March 2003 and April 2018, 1–2 months later than shallow soil water
235 above 100cm during the two droughts. In addition, both the amplitude and frequency
236 of water content variations in the 100–289 cm soil later were remarkably lower than
237 those seen in the upper 100 cm (Fig. 3a, c).

238 As a key physiological structure of trees to absorb soil moisture, the root vertical
239 distribution is directly related to tree's water supply status and closely linked with
240 canopy height (Schenk et al. 2002). Therefore, we used root depth dataset provided by
241 Fan et al. (2017) to investigate the root depth distribution of our sample points. Taller
242 trees have not only deeper roots, but also a larger proportion of deeper roots (Fig. 3b,
243 d), which allows them to buffer drought stress by absorbing water from deeper soil
244 (Giardina et al. 2018; Martínez-Vilalta et al. 2017; Nepstad et al. 1994). For trees taller
245 than 30 m, about 63.3% (2003) and 48.4% (2018) of their roots were distributed below
246 2.89 m, facilitating a stable moisture supply from the deeper soil, which led to a lagged
247 and reduced loss of their greenness. In contrast, more than 40% of <10m trees
248 developed root systems within the upper 100 cm of the soil, thus the rapid water loss

from this near-surface soil could potentially lead to their greater browning (Table S2). However, it is also worth noting that shallow soil is more easily replenished by precipitation, and this favors the faster recovery of shorter trees with shallower root systems. This phenomenon may explain why the mortality of small trees tends to peak in the early stage of droughts (Stovall et al. 2019), whereas for tall trees, peak mortality tends to occur later during periods of prolonged drought (Bigler et al. 2007).

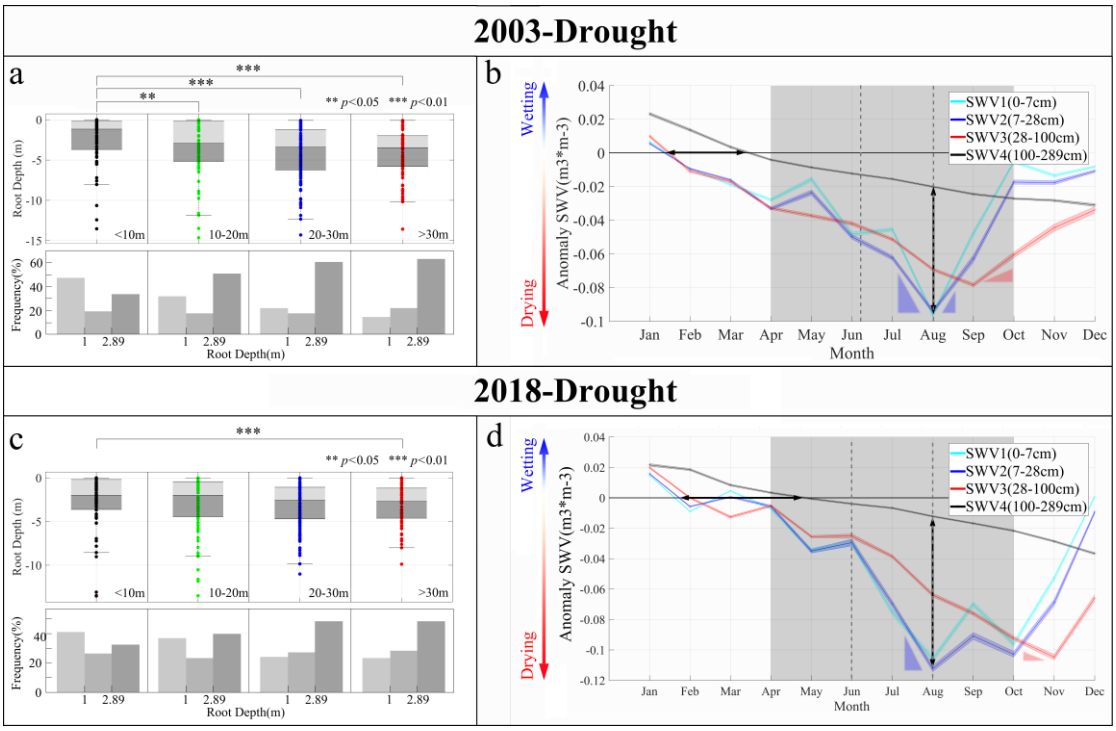

Fig. 3 a, c Average root depths (boxplot) and proportions at different soil depths (histogram) of four height classes: <10 m (black), 10–20 m (green), 20–30 m (blue), and >30 m (red) in the study area. Differences in root depth between different height classes are also shown. The significance of the differences was calculated using a *t* test with significance levels of 0.05 (**) and 0.01 (***). **b, d Average volumetric soil water content anomalies for four soil-depth ranges for time series from 2003 and 2018: 0–7 cm (cyan solid line), 7–28 cm (blue solid line), 28–100 cm (red solid line), and 100–289 cm (black solid line).** Shaded error regions around each curve are standard deviations. Gray shaded regions show the duration (April to October) of the droughts in 2003 and 2018. Horizontal and vertical two-way arrows show the response time lag and the decreased extent, respectively.

3.4 Height-dependence of tree's hydraulic regulating behavior to drought

During drought events, reduced precipitation leads to declines in soil moisture, and this is accompanied by higher temperature and increased evaporation demand from the

atmosphere (Garciaherrera et al. 2010; Liu et al. 2020; Teuling et al. 2006). These environmental factors together stimulate hydraulic regulation behaviors in trees, including reduced stomatal conductance to suppress transpiration, and improved hydraulic conductance in the xylem to transport more moisture from roots to leaves (Giardina et al. 2018; Gimenez et al. 2013; Konings et al. 2017; McDowell et al. 2008). To quantify the height-dependence of the hydraulic regulation capacity of the trees, we used a sapflow density dataset to examine variations in stomatal conductance as the droughts evolved (Phillips et al. 1998; Poyatos et al. 2016). We used data from two forest survey sites with different canopy heights, i.e., FRA_HES_HE2_NON in France and DEU_STE_2P3 in Germany, which recorded the sapflow density variations during the drought of 2003 (Fig. 4).

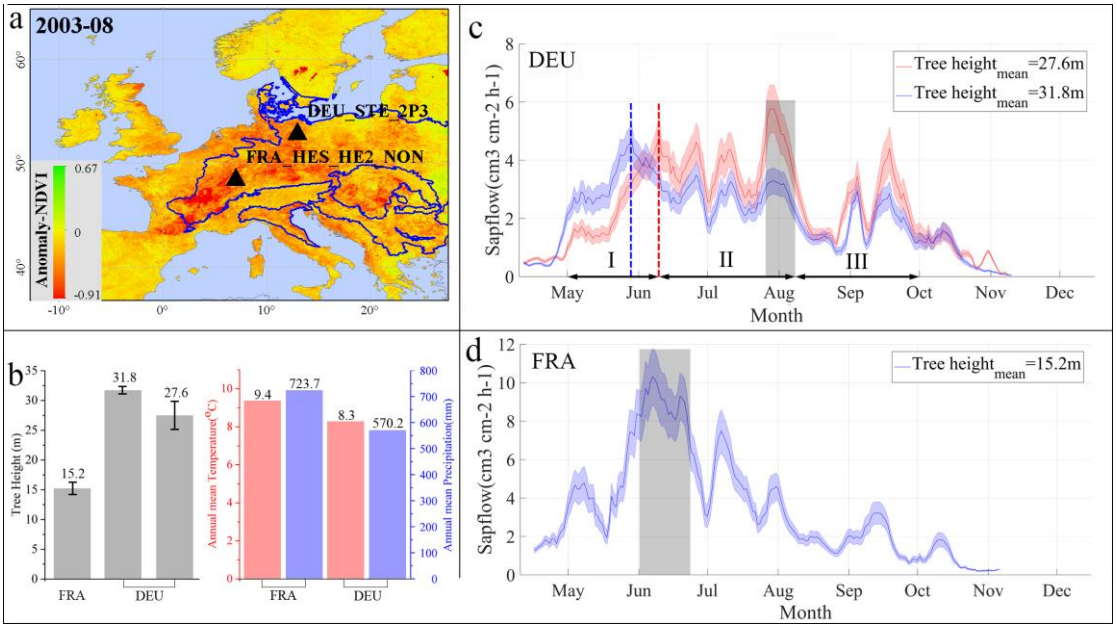

Fig. 4 Sapflow site description and mean daily sapflow density (per cm^2 of sapwood cross-sectional area) during 2003. a. NDVI anomalies distribution in August 2003 and selected site information. b, The average tree height and annual mean temperature and precipitation at the two forest survey sites. c, d Evolution of sapflow density for two forest survey sites. The trees in DEU sites are divided into two groups (red: shorter, blue: taller) according to their height. The sapflow for each group is averaged. A 5-day running average was applied to the sapflow data to improve readability. Shaded error regions are standard deviations. The gray shaded region shows the peak sapflow density during the two distinct periods of exceptional heat that occurred in 2003. The blue and red dashed lines demonstrate the lag effect of stomatal regulation.

The sapflow density of trees at both sites showed an increasing trend during the stage I, indicating that trees optimize stomatal conductance for photosynthesis, which explained the greening-up in the stage I. The exceptional heat in June (García-Herrera et al. 2010) did not significantly increase the sapflow density of trees in site DEU, but instead showed decline trend. This suggests that trees can close stomata to reduce transpiration and to avoid excessive water consumption. From June to August, sapflow density stayed with a steady fluctuation (Fig. 4c). However, there are some differences between tall and short trees. The decline in the sapflow density of taller trees (31.8m) occurred earlier than shorter trees (27.6m) in stage I and maintained a lower sapflow density peak in August, indicating their greater stomatal adjustment ability with respect to buffering environmental evaporation demand (Hubbard et al. 1999; Konings et al. 2017). The earlier decline in the sapflow density of taller trees supports previous works that found that stomatal conductance declines more quickly with the air saturation deficit in old trees than in young trees because older trees show lower conductance over the entire summer to avoid water loss (Giardina et al. 2018; Hubbard et al. 1999). However, the stomatal closure during drought is highly likely to increase the mortality risk of tall trees because it leads to the excessive consumption of carbon (McDowell et al. 2008; West et al. 1999). In contrast, the sapflow density of short trees (site FRA, 15.2m) significantly raises up to its peak value (10.3 ± 1.3 cm-3 cm–2 h–1), indicating stronger transpiration (Gimenez et al. 2013), and the exacerbating consumption of soil water and stem stored water, and eventually contributing to the serious browning of short trees in August.

Tree-scale isohydricity reflects the degree to which a tree can regulate leaf water potential while environmental conditions are drying (Konings et al. 2017). Anisohydricity is the converse of isohydricity, and refers to large variations in leaf

water potential. The weak but significantly negative relationship between anisohydricity and tree height (Fig. S8b) is consistent with the observation that taller trees tend to close their stomata during drought periods to maintain a relatively constant leaf water potential as the soil water potential decreases and atmospheric conditions dry (Giardina et al. 2018; McDowell et al. 2008). In general, taller trees implement a strict regulation strategy between water absorption and loss to resist drought (McDowell et al. 2008).

4. Conceptual framework for height-dependent resistance of trees during drought

Drought accompanied by global warming induced high temperatures is likely to be a widespread environmental stress that will affect forest productivity in the future. Here, we present a process-based schematic diagram (Fig. 5) to crystallize our understanding of the three-stage response of trees to this kind of drought disturbance, and the hydraulic regulation via water absorbing, conducting, and transpiring mechanisms.

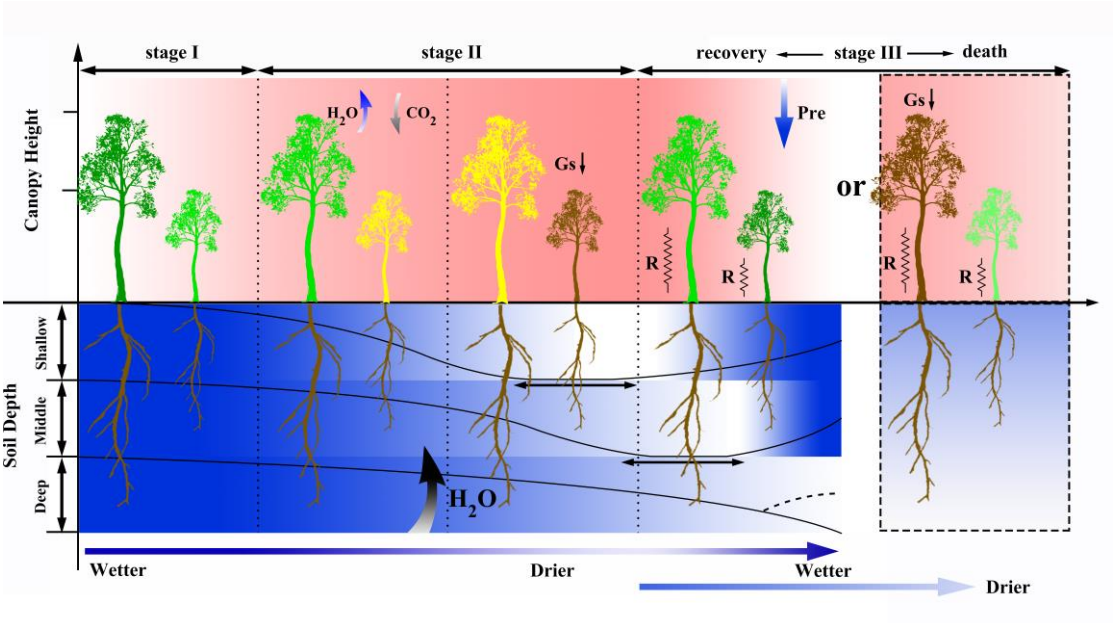

Fig. 5 Schematic diagram showing response of tree activity in different height classes to drought. The response of trees of different heights as the drought intensifies (color of trees and red gradient above the X-axis) and the trend (black solid curve and blue gradient below X-axis) of soil moisture in different soil depths (shallow, middle, deep) changes with the intensification of the drought. During the transition of soil water

conditions from wet to dry (bottom blue gradient arrow), which is typical for a drought, different stages can be distinguished that reflect the different responses of trees of different heights and root depths, and we refer to these as stages I, II, and III. The color of trees reflects the degree of greening or browning. The smaller arrow indicates the different physiological functions: photosynthesis (H_2O: blue gradient up arrow, CO_2: gray gradient down arrow), Gs (stomatal conductance), precipitation (blue gradient down arrow), root water uptake (black gradient up arrow) and R (water transport resistance).

Stage I (Early stage: Greening-up). When the soil water status is adequate and atmospheric evaporative demand is low, increased temperature initiates green-up of the trees (Zaitchik et al. 2006). Taller trees show a greater degree of greening for maximization of light interception to rapid grow (Gimenez et al. 2013). The root system and fully opened stomata maintain the uplift of water from the soil to the leaves, ensuring optimal rates of photosynthesis (Gimenez et al. 2013; Hsiao 1973). A steady increase in sapflow density demonstrates the better hydraulic conductance and increased water-use demand for trees of all heights.

Stage II (Aggravating stage: Browning). As the vapor pressure deficit increases and the soil continues to dry, there is less available soil water for root uptake, particularly for shorter trees with shallow root systems. Combined with the dramatic green-up in the previous stage, which aggravates the water deficit, short trees exhibit rapid and severe browning, and use leaf shedding to mitigate water stress to the remaining foliage. In contrast, benefiting from their deeper roots, tall trees are able to access the relatively steady and plentiful moisture stored in the deeper soil to effectively buffer the water scarcity in the near-surface soil (Brienen et al. 2017; Dawson 1996; Giardina et al. 2018; McDowell et al. 2008; Stovall et al. 2019; Vicente-Serrano et al. 2013). Taller trees also exert a more effective hydraulic regulation capacity, by maintaining steady and low sapflow density and strict isohydricity between stomatal and xylem conductance (Figs 4 and S5), before the continued drought leads to hydraulic failure (Hubbard et al. 1999;

Konings et al. 2017; McDowell et al. 2008). As a consequence, taller trees exhibit a hysteretic and less pronounced browning during extreme drought events.

Stage III (Recovery). With the decrease in air temperature and the return of precipitation, the water deficit experienced by the trees is relieved and recovery begins. The shallow roots and shorter water transport path of shorter trees encourage the rapid uptake of water and a quicker recovery (Stovall et al. 2019; West et al. 1999). The recovery of the taller trees is limited by factors such as delays to the recharge of water in the deeper soil (Dawson et al. 1996; Fan et al. 2017), interception of soil water by shallower roots (Cannon 1911; Fan et al. 2017; Zipper et al. 2015), longer water uplift and transport pathways (Martínez-Vilalta & Garcia-Forner 2017; Martínez-Vilalta et al. 2014), and finally, possible physiological changes associated with drought-induced stomatal closure. Low rates of photosynthesis caused by stomatal closure can lead to depletion of non-structural carbohydrate pools (McDowell et al. 2008; Stovall et al. 2019) and also damage to hydraulic pathways including the reversible collapse of leaf veins, regulation of aquaporins in cell membranes, and the formation of cortical lacunae in the fine roots (Choat et al. 2018). Thus, the recovery of tall trees is a relatively slower functional reviving process. In other scenarios of persistent drought and deep soil water deficit could not be alleviated, the hydraulic regulation at the previous stage may increases the risk of carbon starvation (Sevanto et al. 2014), thus increasing mortality risk for tall trees (Stovall et al. 2019).

In general, tree height was the strongest predictor of tree response during drought, in that it leads to different strategies by which trees attempt to cope with drought stress. Trees optimize their root systems, leaf stomata, and xylem tissue to form a balance between limiting the loss of water and allowing maximal photosynthesis subject to

388 water availability (Cowan et al. 1977; Manzoni et al. 2011; Medlyn et al. 2011). Trees
389 adjust their water regulation strategy as they grow taller and age, and inherit species-
390 specific hydraulic traits adapted for specific environments.

391 **5. Conclusions**

392 Devastating droughts are becoming more frequent in Europe and are already having
393 significant impacts on the forest structure and function. In this study, we examined the
394 phenomenal and hydraulic response of trees to droughts, focused on the height-
395 dependent behavior of trees during the drought evolution process. We defined three
396 stages of a drought event based on the greenness of trees: early (green-up), middle
397 (browning), and post (recovery). Our observations illustrate that shorter trees are more
398 vulnerable to shorter, more intense droughts; however, they are more likely to recover
399 than taller trees after droughts. Shorter trees are more sensitive to water condition
400 variations, including water deficit and water recovery. Although taller trees are more
401 resistant to short, intense droughts, a prolonged water deficit likely cause more serious
402 damage to taller trees. Root systems and stomata are important physiological structural
403 controls on the balance between water loss and gain, and it is this balancing behavior
404 that drives the height-dependent resistance of forests to drought stress.

405 We have demonstrated in this work how the differences in structure affect the response
406 of tall and short trees to water availability at each stage of a drought, and also shown
407 the response of these different physiological mechanisms to the intensity and duration
408 of water stress. The natural succession and anthropogenic deforestation are likely to
409 alter the forest structure and also the hydraulic traits that help to resist heatwaves and
410 droughts. Process-based vegetation models require to incorporate the hydraulic-trait

dynamics of trees under water-limiting conditions if we are to improve our understanding of the resilience of forests under future climate change.

Acknowledgements

This work was supported by the Strategic Priority Research Program of the Chinese Academy of Sciences (grant no. XDA20060402), the National Key Scientific Research and Development Program of China (grant no. 2018YFC1509003), and the Second Tibetan Plateau Scientific Expedition and Research Program (grant No. 2019QZKK0906). The forest canopy height dataset was obtained from the NASA Carbon Monitoring System (CMS) program (https://daac.ornl.gov/cgi-bin/dsviewer.pl?ds_id=1271). The ERA5 reanalysis datasets were provided by the European Centre for Medium Range Weather Forecasts (ECMWF; https://cds.climate.copernicus.eu/cdsapp#!/data-set/reanalysis-era5-single-levels?tab=form). The precipitation dataset was obtained from the Climate Research Unit (CRU). (http://data.ceda.ac.uk// badc/cru/). The normalized difference vegetation index (NDVI) and enhanced vegetation index (EVI) were obtained from the Moderate Resolution Imaging Spectroradiometer (http://modis.gsfc.nasa.gov/). The sapflow density dataset was obtained from sap flow measurements (SAPFLUXNET: https://zenodo.org/record/ 3697807#. Xs4yo4gza5u). The global map of forest tree density was obtained from (Crowther et al. 2015) https://elischolar.library.yale.edu/yale_fes_data/1/?tdsourcetag=s_pctim_aiomsg). The global maximum rooting depth of forests was obtained from Fan et al. (2017) https://wci.earth2observe.eu/thredds/catalog/usc/root-depth/catalog.html). The degrees of isohydricity metrics showing the differences in the tree stomatal regulation.at the ecosystem scale were obtained from (Konings et al., 2017) http://github.com/agkonings/isohydricity).

436 **References**

437 Allen, C. D., Macalady, A. K., Chenchouni, H., Bachelet, D., McDowell, N., Vennetier,
438 M., et al. (2010). A global overview of drought and heat-induced tree mortality
439 reveals emerging climate change risks for forests. *Forest Ecology and Management*,
440 259(4), 660-684.

441 Bennett, Mcdowell, Allen, & Andersonteixeira. (2015). Larger trees suffer most during
442 drought in forests worldwide. *Nature Plants*, 1(10), 15139-15139.

443 Bennett, A. C., McDowell, N. G., Allen, C. D., & Anderson-Teixeira, K. J. (2015).
444 Larger trees suffer most during drought in forests worldwide. *Nature Plants*, 1(10),
445 15139.

446 Bevan, S., Los, S., & North, P. (2014). Response of vegetation to the 2003 European
447 drought was mitigated by height. *Biogeosciences*, 11(11).

448 Bovard, B. D., Curtis, P. S., Vogel, C. S., Su, H., & Schmid, H. P. (2005).
449 Environmental controls on sap flow in a northern hardwood forest. *Tree physiology*,
450 25(1), 31-38.

451 Brienen, R., Gloor, E., Clerici, S., Newton, R., Arppe, L., Boom, A., et al. (2017). Tree
452 height strongly affects estimates of water-use efficiency responses to climate and CO
453 2 using isotopes. *Nature communications*, 8(1), 1-10.

454 Cannon, W. A. (1911). The root habits of desert plants: Carnegie Institution of
455 Washington.

456 Choat, B., Brodribb, T. J., Brodersen, C. R., Duursma, R. A., Lopez, R., & Medlyn, B.
457 E. (2018). Triggers of tree mortality under drought. *Nature*, 558(7711), 531-539.

458 Ciais, P., Reichstein, M., Viovy, N., Granier, A., Ogée, J., Allard, V., et al. (2005).
459 Europe-wide reduction in primary productivity caused by the heat and drought in
460 2003. *Nature*, 437(7058), 529-533.

461 Crowther, T. W., Glick, H. B., Covey, K. R., Bettigole, C., Maynard, D. S., Thomas, S.
462 M., et al. (2015). Mapping tree density at a global scale. *Nature*, 525(7568), 201-205.

463 Dawson, T. E. (1996). Determining water use by trees and forests from isotopic, energy
464 balance and transpiration analyses: the roles of tree size and hydraulic lift. *Tree*
465 *physiology*, 16, 263-272.

466 Dawson, T. E., & Pate, J. (1996). Seasonal water uptake and movement in root systems
467 of Australian phraeatophytic plants of dimorphic root morphology: a stable isotope
468 investigation. *Oecologia*, 107(1), 13-20.

469 Dixon, R. K., Solomon, A., Brown, S., Houghton, R., Trexier, M., & Wisniewski, J.
470 (1994). Carbon pools and flux of global forest ecosystems. *Science*, 263(5144), 185-
471 190.

472 Fan, Y., Miguez-Macho, G., Jobbágy, E. G., Jackson, R. B., & Otero-Casal, C. (2017).
473 Hydrologic regulation of plant rooting depth. *Proceedings of the national academy*
474 *of sciences*, 114(40), 10572-10577.

Fischer, E. M., & Schär, C. (2010). Consistent geographical patterns of changes in high-impact European heatwaves. *Nature Geoscience*, 3(6), 398-403.

Fischer, E. M., Seneviratne, S. I., Vidale, P. L., Lüthi, D., & Schär, C. (2007). Soil moisture–atmosphere interactions during the 2003 European summer heat wave. *Journal of Climate*, 20(20), 5081-5099.

García-Herrera, R., Díaz, J., Trigo, R. M., Luterbacher, J., & Fischer, E. M. (2010). A review of the European summer heat wave of 2003. *Critical Reviews in Environmental Science and Technology*, 40(4), 267-306.

Garciaherrera, R., Diaz, J., Trigo, R. M., Luterbacher, J., & Fischer, E. M. (2010). A Review of the European Summer Heat Wave of 2003. *Critical Reviews in Environmental Science and Technology*, 40(4), 267-306.

Giardina, F., Konings, A. G., Kennedy, D., Alemohammad, S. H., Oliveira, R. S., Uriarte, M., et al. (2018). Tall Amazonian forests are less sensitive to precipitation variability. *Nature Geoscience*, 11(6), 405-409.

Gimenez, C., Gallardo, M., & Thompson, R. (2013). Plant–Water Relations.

Healey, S., Hernandez, M., Edwards, D., Lefsky, M., FREEMAN, J., Patterson, P., et al. (2016). CMS: GLAS LiDAR-Derived Global Estimates of Forest Canopy Height, 2004-2008. ORNL DAAC.

Hsiao, T. C. (1973). Plant Responses to Water Stress. *Annual Review of Plant Biology*, 24(1), 519-570.

Hubbard, R. M., Bond, B. J., & Ryan, M. G. (1999). Evidence that hydraulic conductance limits photosynthesis in old Pinus ponderosa trees. *Tree physiology*, 19(3), 165-172.

Ji, L., & Peters, A. J. (2003). Assessing vegetation response to drought in the northern Great Plains using vegetation and drought indices. *Remote Sensing of Environment*, 87(1), 85-98. doi:https://doi.org/10.1016/S0034-4257(03)00174-3

Kogan, F. (1997). Global Drought Watch from Space. *Bulletin of the American Meteorological Society*, 78(4), 621-636.

Kogan, F. N. (1995). Application of vegetation index and brightness temperature for drought detection. *Advances in space research*, 15(11), 91-100.

Konings, A. G., Gentine, P., & Ga. (2017). Global variations in ecosystem‐scale isohydricity. *Glob Chang Biol*, 23(2), 891-905.

Lüttschwager, D., & Remus, R. (2007). Radial distribution of sap flux density in trunks of a mature beech stand. *Annals of forest science*, 64(4), 431-438. doi:10.1051/forest:2007020

Lefsky, M. A., Keller, M., Pang, Y., De Camargo, P. B., & Hunter, M. O. (2007). Revised method for forest canopy height estimation from Geoscience Laser Altimeter System waveforms. *Journal of Applied Remote Sensing*, 1(1), 013537.

Liberto, T. D. (2018). A hot, dry summer has led to drought in Europe in 2018. ClimateWatch Magazine, Retrieved from https://www.climate.gov/news-features/event-tracker/hot-dry-summer-has-led-drought-europe-2018.

Lindenmayer, D. B., Laurance, W. F., & Franklin, J. F. (2012). Global Decline in Large Old Trees. *Science*, 338(6112), 1305-1306.

Liu, He, B., Guo, L., Huang, L., & Chen, D. (2020). Similarities and Differences in the Mechanisms Causing the European Summer Heatwaves in 2003, 2010, and 2018. *Earth's Future*.

Liu, W. T., & Kogan, F. N. (1996). Monitoring regional drought using the Vegetation Condition Index. *International Journal of Remote Sensing*, 17(14), 2761-2782. doi:10.1080/01431169608949106

Lutz, J. A., Larson, A. J., Swanson, M. E., & Freund, J. A. (2012). Ecological importance of large-diameter trees in a temperate mixed-conifer forest. *PLoS ONE*, 7(5).

Martínez-Vilalta, J., & Garcia-Forner, N. (2017). Water potential regulation, stomatal behaviour and hydraulic transport under drought: deconstructing the iso/anisohydric concept. *Plant, cell & environment*, 40(6), 962-976.

Martínez-Vilalta, J., Poyatos, R., Aguadé, D., Retana, J., & Mencuccini, M. (2014). A new look at water transport regulation in plants. *New phytologist*, 204(1), 105-115.

McDowell, N., Pockman, W. T., Allen, C. D., Breshears, D. D., Cobb, N., Kolb, T., et al. (2008). Mechanisms of plant survival and mortality during drought: why do some plants survive while others succumb to drought? *New Phytologist*, 178(4), 719-739.

McDowell, N. G., & Allen, C. D. (2015). Darcy's law predicts widespread forest mortality under climate warming. *Nature Climate Change*, 5(7), 669-672.

Meehl, G. A., & Tebaldi, C. (2004). More intense, more frequent, and longer lasting heat waves in the 21st century. *Science*, 305(5686), 994-997.

Nepstad, D. C., De Carvalho, C. J. R., Davidson, E. A., Jipp, P. H., Lefebvre, P., Negreiros, G., et al. (1994). The role of deep roots in the hydrological and carbon cycles of Amazonian forests and pastures. *Nature*, 372(6507), 666-669.

Nepstad, D. C., Tohver, I. M., Ray, D., Moutinho, P., & Cardinot, G. (2007). Mortality of large trees and lianas following experimental drought in an amazon forest. *Ecology*, 88(9), 2259-2269.

Painho, M., Farral, H., & Barata, F. (1996). Digital map of European ecological regions (DMEER). Its concept and elaboration. Paper presented at the Proceedings of the second joint European conference & exhibition on Geographical information (Vol. 1) : from research to application through cooperation: from research to application through cooperation, Barcelona, Spain.

Pan, Y., Birdsey, R., Phillips, O. L., & Jackson, R. B. (2013). The Structure, Distribution, and Biomass of the World's Forests. *Annual Review of Ecology, Evolution, and Systematics*, 44(1), 593-622.

Peters, A. J., Walters hea, E. A., Ji, L., Vina, A., Hayes, M. J., & Svoboda, M. (2002). Drought Monitoring with NDVI-Based Standardized Vegetation Index. *Photogrammetric Engineering and Remote Sensing*, 68(1), 71-75.

Phillips, N., & Oren, R. (1998). A comparison of daily representations of canopy conductance based on two conditional time-averaging methods and the dependence of daily conductance on environmental factors. *Annales des Sciences Forestieres*.

Phillips, O. L., Der Heijden, G. M. F. V., Lewis, S. L., Lopezgonzalez, G., Aragao, L. E. O. C., Lloyd, J., et al. (2010). Drought–mortality relationships for tropical forests. *New phytologist*, 187(3), 631-646.

Poyatos, R., Granda, V., Molownyhoras, R., Mencuccini, M., Steppe, K., & Martinezvilalta, J. (2016). SAPFLUXNET: towards a global database of sap flow measurements. *Tree physiology*, 36(12), 1449-1455.

Ryan, M. G., Binkley, D., & Fownes, J. H. (1997). Age-related decline in forest productivity : Pattern and process. *Advances in Ecological Research*, 27, 213-262.

Ryan, M. G., & Yoder, B. J. (1997). Hydraulic limits to tree height and tree growth. *Bioscience*, 47(4), 235-242.

Schär, C., Vidale, P. L., Lüthi, D., Frei, C., Häberli, C., Liniger, M. A., et al. (2004). The role of increasing temperature variability in European summer heatwaves. *Nature*, 427(6972), 332-336.

Schenk, H. J., & Jackson, R. B. (2002). Rooting depths, lateral root spreads and below-ground/above-ground allometries of plants in water-limited ecosystems. *Journal of Ecology*, 90(3), 480-494.

Seneviratne, S. I., Lüthi, D., Litschi, M., & Schär, C. (2006). Land–atmosphere coupling and climate change in Europe. *Nature*, 443(7108), 205-209.

Sevanto, S., Mcdowell, N. G., Dickman, L. T., Pangle, R., & Pockman, W. T. (2014). How do trees die? A test of the hydraulic failure and carbon starvation hypotheses. *Plant, cell & environment*, 37(1), 153-161.

Stovall, Shugart, H. H., & Yang, X. (2019). Tree height explains mortality risk during an intense drought. *Nat Commun*, 10(1), 4385. doi:10.1038/s41467-019-12380-6

Stovall, Shugart, H. H., & Yang, X. (2020). Reply to "Height-related changes in forest composition explain increasing tree mortality with height during an extreme drought". *Nat Commun*, 11(1), 3401. doi:10.1038/s41467-020-17214-4

Stovall, A. E., Shugart, H., & Yang, X. (2019). Tree height explains mortality risk during an intense drought. *Nature communications*, 10(1), 1-6.

Teuling, A. J., Uijlenhoet, R., Hupet, F., & Troch, P. A. (2006). Impact of plant water uptake strategy on soil moisture and evapotranspiration dynamics during drydown. *Geophysical Research Letters*, 33(3).

Vicente-Serrano, S. M., Gouveia, C., Camarero, J. J., Beguería, S., Trigo, R., López-Moreno, J. I., et al. (2013). Response of vegetation to drought time-scales across

592 global land biomes. *Proceedings of the National Academy of Sciences*, 110(1), 52-
593 57.

594 Vince, A. (2002). A framework for the greedy algorithm. *Discrete Applied Mathematics*,
595 121(1), 247-260.

596 West, G. B., Brown, J. H., & Enquist, B. J. (1999). A general model for the structure
597 and allometry of plant vascular systems. *Nature*, 400(6745), 664.

598 Xu, P., Zhou, T., Yi, C., Luo, H., Zhao, X., Fang, W., et al. (2018). Impacts of Water
599 Stress on Forest Recovery and Its Interaction with Canopy Height. *International*
600 *Journal of Environmental Research and Public Health*, 15(6), 1257.

601 Zaitchik, B. F., Macalady, A. K., Bonneau, L. R., & Smith, R. B. (2006). Europe's 2003
602 heat wave: a satellite view of impacts and land–atmosphere feedbacks. International
603 Journal of Climatology: *A Journal of the Royal Meteorological Society*, 26(6), 743-
604 769.

605 Zhang, Y., Meinzer, F. C., Hao, G., Scholz, F. G., Bucci, S. J., Takahashi, F. S. C., et
606 al. (2009). Size-dependent mortality in a Neotropical savanna tree: the role of height-
607 related adjustments in hydraulic architecture and carbon allocation. *Plant Cell and*
608 *Environment*, 32(10), 1456-1466.

609 Zipper, S. C., Soylu, M. E., Booth, E. G., & Loheide, S. P. (2015). Untangling the
610 effects of shallow groundwater and soil texture as drivers of subfield‐scale yield
611 variability. *Water Resources Research*, 51(8), 6338-6358.

612